Electron Transfer Involving Nonbonded Superexchange Interactions in Rigid Donor−Acceptor Arrays†

Aaron S. Lukas, Patrick J. Bushard, and Michael R. Wasielewski*

Department of Chemistry and Center for Nanofabrication and Molecular Self-Assembly, Northwestern University, Evanston, Illinois 60208-3113

Received: June 19, 2001; In Final Form: September 26, 2001

Rigid intramolecular Donor−Acceptor(1)⌐Acceptor(2)−X trichromophoric arrays based on a 4,5-diaminoxanthene bridge B were prepared in which the xanthene bridge orients A_2 relative to D, so that nonbonded interactions between ^{1}*D and A_2 can be studied. The electron donor, D, is 4-(*N*-piperidinyl)naphthalene-1,8-dicarboximide (ANI), and the acceptors A_1 and A_2 are pyromellitimide (PI) and naphthalene-1,8:4,5-bis-(dicarboximide) (NI), respectively, and X is either *n*-C_8H_{17} or H. The torsional angles of the xanthene−imide single bonds orient the NI and PI acceptors approximately cofacial to one another. Femtosecond transient absorption measurements show that electron transfer from ^{1}*ANI to NI occurs by nonbonded superexchange interactions that include contributions from both the *n*-C_8H_{17} substituent on the NI acceptor and nearby solvent molecules. The structural rigidity of these compounds allows evaluation of the distance dependence of both charge separation and recombination. For charge separation, $\beta = 1.1-1.3$ Å^{-1}, and evidence exists for solvent contributions to superexchange in BzCN. The distance dependence of the charge recombination rates also correlates strongly with contributions from solvent molecules mediating this process via a hole-transfer mechanism in toluene, where $\beta = 0.3$ Å^{-1}. Our findings indicate that mediation of electron transfer by nonbonded interactions can compete effectively with electron transfer via bonded pathways.

Introduction

The bacterial photosynthetic reaction center has been studied extensively due to its ability to convert light energy into chemical potential with near unity quantum yield.[1] The primary charge separation (CS) events result in electron transfer from the lowest excited state of a bacteriochlorophyll dimer (P) to a bacteriopheophytin (H) across 17 Å in about 3.5 ps. The mechanism of this reaction is of considerable interest due to its high efficiency and the role played by the bridging bacteriochlorophyll (BChl), which is positioned between P and H.[1−6] Recent discussions in the literature differentiate between a two-step, sequential mechanism through a P^+-BChl^--H intermediate, and a superexchange mechanism in which a virtual P^+-BChl^--H state participates.[7−10] At ambient temperature, transient absorption spectroscopy provides conclusive evidence that P^+-BChl^--H is a real intermediate that forms with $\tau_{CS} = 3.5$ ps, and whose concentration is limited by a rapid $P^+-BChl^--H \rightarrow P^+-BChl\text{-}H^-$ charge shift with $\tau_{CS} = 0.9$ ps.[3]

Electron transfer within the bacterial photosynthetic reaction center relies on a complex set of electronic coupling matrix elements arising from covalent and noncovalent orbital interactions, the overall sum of which results in highly efficient charge separation. Subtle structural and energetic differences between the A and B branches of the reaction center result in preferential CS down only the A branch of the system. For example, crystal structures of the reaction center show that one of the phytyl chains on the A-side of the special pair lays in a groove between the BChl and H, while that on the B-side of the reaction center does not.[11,12] However, the dense packing of chromophores makes isolation of the contribution of the phytyl chain to the electronic coupling difficult.[11,12]

Numerous model compounds have been synthesized to experimentally test superexchange mechanisms mediated by both bonded and nonbonded pathways. Bridge mediated electron transfer has been studied in rigid and semirigid arrays of porphyrin[13−15] and chlorophyll[16−19] chromophores covalently linked to various acceptors. By mimicking the spatial arrangement of chromophores within the reaction center and systematically changing their electronic properties, both superexchange[20−22] and sequential[23,24] ion pair formation mechanisms have been demonstrated.

More recently, researchers have synthesized structures that allow a through-medium pathway to take precedence over bonded interactions. These D−B−A compounds attempt to quantify "through-space"[25−31] or "solvent-mediated"[26,32−37] electronic coupling contributions to ET rates. In these compounds, superexchange mediated electron transfer occurs via nonbonded pathways involving either solvent molecules or peripheral functional groups. Additionally, porphyrin systems with facial and axially appended acceptor groups have been synthesized.[38−41] Zimmt and co-workers have found that the placement of solvent molecules in a cleft between the donor and acceptor molecules significantly enhances ET rates both by relaxing symmetry restrictions on these processes, and by contributing low-lying orbitals for superexchange. Electron-transfer rates reflect the vertical energy gap between the ^{1}*D excited state and the $D^+-solvent^--A$ virtual state, and can be related to the vertical electron affinity[42] of the solvent.[32,33] Other groups have synthesized U-shaped triads and tetrads with longer bridges in which specific binding sites are located for solvent

† Part of the special issue "Noburo Mataga Festschrift".

* To whom correspondence should be addressed. E-mail: wasielew@chem.northwestern.edu.

10.1021/jp012309q CCC: $22.00
Published on Web 11/30/2001

molecules to bind.[35] In these systems different isomeric norbornane bridges significantly affect the photophysical properties of D−A dyads, leading to varying contributions from through-bond and through-medium electronic coupling.[34,36]

Our interest in superexchange mediated electron-transfer mechanisms has led us to prepare a series of rigid intramolecular

Donor-Acceptor(1)┐
Bridge
X-Acceptor(2)┘

trichromophoric arrays based on a 4,5-diaminoxanthene[43] bridge, **1**−**6**, where X = *n*-C_8H_{17} and H. In these molecules the

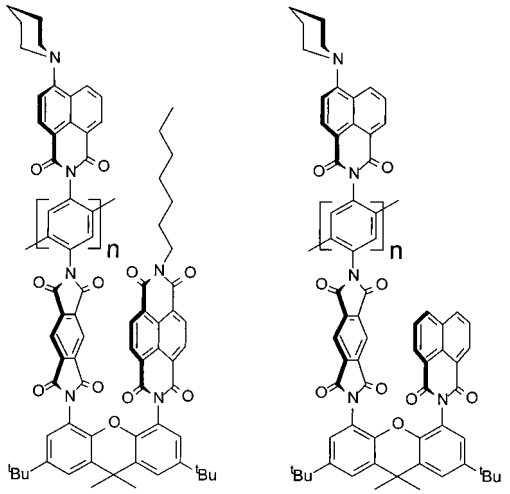

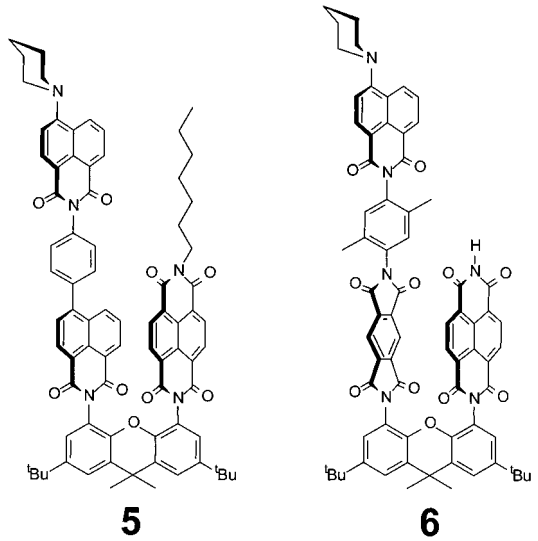

xanthene spacer is used to orient A_2 relative to D, so that nonbonded interactions between ^{1}*D and A_2 can be studied. Apart from the trivial case of a sequential electron-transfer mechanism involving real intermediates, electron transfer from ^{1}*D to A_2 can occur by the three main pathways shown in Scheme 1. The through-bond pathway (A) between ^{1}*D and A_2 in the molecules studied here is by design much too long to allow CS to occur in competition with excited-state decay of ^{1}*D. In pathway B, electron transfer may occur by direct orbital overlap between ^{1}*D and A_2, a so-called through-space interaction. Last, in pathway C, electron transfer can occur by means of a superexchange interaction involving the orbitals of substituents X of A_2 that are close to ^{1}*D, yet are not directly bonded to it. This is similar to the role that the phytyl group of the bacteriochlorophylls and bacteriopheophytins in the photosynthetic reaction center may play in assisting electron transfer.[11,12] In addition, superexchange involving solvent molecules positioned between ^{1}*D and A_2 may also be considered as a variant of this pathway. Of course, in most molecules several of these electron-transfer pathways operate simultaneously, and the challenge is to factor the contributions of each pathway to the overall electron-transfer rate. In the molecules presented here, rigid structures are developed that allow particular pathways to dominate the overall electron-transfer rate.

SCHEME 1

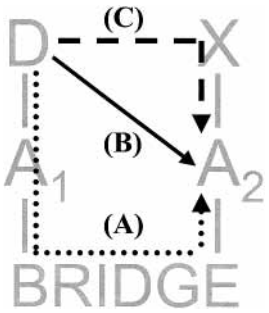

The electron acceptors pyromellitimide (PI) and naphthalene-1,8:4,5-bis(dicarboximide) (NI) are attached to the xanthene bridge through the nitrogen atoms of their imide groups. The torsional angles of the xanthene−imide single bonds orient the NI and PI acceptors approximately cofacial to one another, and result in rigid structures in which the primary degrees of conformational freedom are limited rotations about these bonds through the long axes of the various components of the assembly. In compounds **1**−**4** the electron donor 4-(*N*-piperidinyl)naphthalene-1,8-dicarboximide (ANI) is attached to PI via either an N−N bond which links them directly, or by means of an intervening 2,5-dimethylphenyl spacer. In compounds **1** and **2** the imide of NI that points toward ANI is functionalized with an *n*-C_8H_{17} chain. The results indicate that the primary charge separation event within **1** and **2** is ^{1}*ANI−PI−NI → ANI^+PI−NI^-. The results on compounds **3**−**6** are used to support this finding, and strongly suggest that photoinduced CS is in part mediated by the *n*-C_8H_{17} chain attached to the imide of NI. Specifically, compounds **3** and **4** are dyads in which the electron-transfer dynamics between ANI and PI can be studied in the absence of the NI acceptor. In each molecule NI is replaced with a 1,8-naphthalenemonoimide (NMI), which on an energetic basis cannot be reduced by ^{1}*ANI, but retains the substituent pattern and steric effects of the planar aromatic core of NI. Conversely, compound **5** is a model dyad in which NMI is substituted for PI, and is designed to study electron transfer from ^{1}*ANI to NI when PI is absent. Finally, compound **6** is identical to **2** except that the aliphatic chain at the imide of NI is replaced with an H atom.

Experimental Section

The syntheses of compounds **1**−**6** and all intermediates are presented in detail in the Supporting Information. Characterization was performed with a Varian 400 MHz NMR and a Perseptive BioSystems time-of-flight MALDI mass spectrometer. Femtosecond transient absorption measurements were made using 420 nm, 130 fs, and 1 μJ excitation pulses generated by

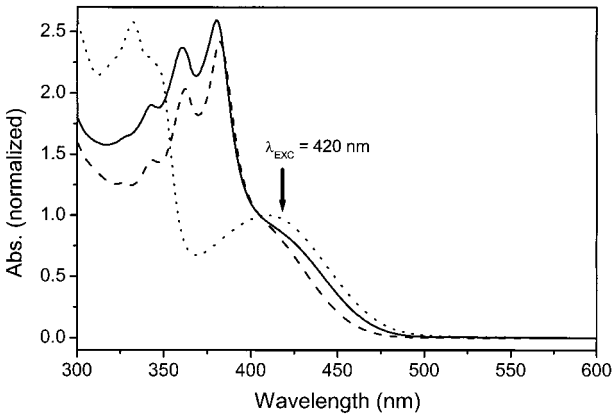

Figure 1. Ground-state electronic absorption spectra of compounds **1** (−), **2** (- - -), and **3** (·····) in toluene.

a frequency-doubled, regeneratively amplified, titanium sapphire laser system operating at a 2 kHz repetition rate and a white light continuum probe pulse generated by focusing the 840 nm fundamental into a sapphire disk. The total instrument response is 180 fs. Nanosecond transient absorption measurements were carried out using 6 ns, 416 nm, and 1 mJ pulses generated by Raman shifting in H_2 the output from a frequency-tripled Nd:YAG laser operating at a 10 Hz repetition rate. A 60 μs Xe flash lamp (EG&G FX215) pulse was used as the tunable probe pulse. The total instrument response is 7 ns. Both laser systems have been described in detail elsewhere.[44] Cuvettes having 2 and 10 mm path lengths were used for the femtosecond and nanosecond experiments, respectively, while the optical densities of the samples at the excitation wavelengths were maintained at 0.3−0.8. Steady-state absorption and emission spectra were obtained using a Shimadzu 1601 UV−vis spectrophotometer and a PTI instruments single photon counting fluorimeter. A 10 mm quartz cuvette was used for the fluorescence measurements with a sample optical density of 0.1 ± 0.05 OD at 420 nm to avoid reabsorption artifacts. All solvents were spectrophotometric grade.

Electrochemical measurements were performed in butyronitrile containing 0.1 M *n*-tetrabutylammonium perchlorate electrolyte. A 1.0 mm diameter platinum disk electrode, platinum wire counter electrode, and Ag/Ag_xO reference electrode were employed. The ferrocene/ferrocinium couple (Fc/Fc^+, 0.52 vs SCE) was used as an internal standard for all measurements.

Results

Steady-State Spectroscopy. The photophysics of the 4-(*N*-piperidinyl)naphthalene-1,8-dicarboximide (ANI) chromophore have been characterized previously in detail.[24] Briefly, the ground-state optical spectrum of ANI exhibits a broad absorption centered at 397 nm in toluene, and has significant charge-transfer (CT) character. Figure 1 shows the ground-state spectra of **1**−**3** in toluene. All three molecules display the ANI CT absorption band near 400 nm, while **1** and **2** show the vibronic structure arising from π-π* transitions of the NI acceptor at 343, 363, and 382 nm as well. The ground-state absorption maximum of PI occurs at 307 nm, and cannot be resolved from bands due to ANI and NI, which also absorb in this region. The large absorption band at 340 nm in **3** is due to NMI. The steady-state spectroscopic properties of **1**−**6** in toluene, 2-methyltetrahydrofuran (MTHF), butyronitrile (PrCN), and benzonitrile (BzCN) listed in Table 1 are consistent with the CT nature of the ^{1}*ANI excited state.

TABLE 1: Steady-State Absorption and Fluorescence Data for ANI and 1−6

	toluene				MTHF			
compd	λ_{abs}	λ_{em}	E_S (eV)	Φ_f	λ_{abs}	λ_{em}	E_S (eV)	Φ_f
ANI	397	500	2.80	0.91	397	510	2.77	0.76
1	406	503	2.76	0.007	408	513	2.72	<0.001
2	397	496	2.81	0.18	400	510	2.77	0.071
3	416	514	2.70	0.018	416	521	2.68	0.02
4	398	499	2.80	0.66	400	510	2.76	0.44
5	397	501	2.80	0.052	400	512	2.76	0.011
6	398	500	2.80	0.32	400	510	2.77	0.09

	PrCN				BzCN			
compd	λ_{abs}	λ_{em}	E_S (eV)	Φ_f	λ_{abs}	λ_{em}	E_S (eV)	Φ_f
ANI	406	532	2.69	0.23	414	535	2.66	0.58
1	420	540	2.62	<0.001	427	538	2.60	<0.001
2	404	531	2.70	0.050	414	531	2.66	0.038
3	425	527	2.63	0.023	425	535	2.62	0.013
4	408	523	2.70	0.18	425	525	2.64	0.36
5	405	529	2.70	0.050	414	533	2.66	0.028
6	404	531	2.70	0.09	415	532	2.66	0.04

The ^{1}*ANI excited state decays radiatively and is stabilized in more polar solvents, resulting in red-shifted absorption and emission maxima, and decreased fluorescence quantum yields, Table 1. Direct attachment of two imides via an N−N bond as in **1** and **3** further stabilizes both the ground and excited states of ANI via an electron withdrawing inductive effect, which lowers the energy of ^{1}*ANI by approximately 0.05 eV relative to an *N*-phenyl substituent. Stabilization of ^{1}*ANI by electron withdrawing substituents has been observed in analogous compounds.[45] This is observed in **1** and **3** as a red shift of several nanometers in both the absorption and emission spectra, relative to the other compounds. The ANI absorption and emission maxima within **3** are red shifted to an even greater extent than in **1**, indicative of a stronger interaction between ANI and PI. It is possible that steric crowding between the imides of ANI and NI within **1** increases the dihedral angle between ANI and PI, resulting in diminished interaction between the ANI and PI π systems in **1** relative to that in **3**.

The fluorescence emission from ^{1}*ANI is quenched in the presence of nearby electron acceptors, which is due to photoinduced electron transfer (see below). The fluorescence quantum yields of compounds **1**−**6** are listed in Table 1, and show the strongest degree of quenching within **1** and **3**, while emission from the other compounds is diminished to a lesser extent. The fluorescence emission from **4** is only weakly quenched, indicating that electron transfer is likely not competitive with excited-state decay in this molecule.

Redox Chemistry. The electrochemical properties of aromatic imides and diimides are highly sensitive to the nature of the group attached to the imide nitrogen atom.[46] Imides substituted with electron-withdrawing groups have more positive reduction potentials due to inductive stabilization of the anion radical. Cyclic voltammetry conducted in PrCN containing 0.1 M tetra-*n*-butylammonium perchlorate confirms that the local environment plays a significant role in determining the reduction potentials of PI and NI and the oxidation potential of ANI. The first and second reduction potentials of NI and PI, as well as the oxidation and reduction potential of ANI within compounds **1**−**6** are compiled in Table 2. The first reduction potential of PI is more positive by approximately 0.1 V in compounds **1** and **3** where it is directly linked to the imide of ANI. Likewise, the oxidation potential of the ANI donor within these compounds increases by approximately 0.1 V. Cyclic voltammograms from compounds **1** and **2** are displayed in Figure 2, and show four

TABLE 2: Electrochemical Properties of Compounds 1−6 in Butyronitrile (All Potentials vs SCE)

compd	$E_0^{ANI^+}$	$E_0^{ANI^-}$	$E_0^{NI^-}$	$E_0^{PI^-}$	$E_0^{NI^{-2}}$	$E_0^{PI^{-2}}$
1	1.32	−1.35	−0.48	−0.66	−1.08	−1.22
2	1.24	−1.44	−0.42	−0.75	−1.11	−1.29
3	1.35	−1.35	−0.65	−1.27		
4	1.25	−1.44	−0.74	−1.28		
5	1.16	−1.46	−0.45	−1.09		
6	1.30	−1.44	−0.44	−0.76	−1.16	−1.31

separate reduction waves assigned to the first and second reductions of NI and PI, as well as the oxidation wave assigned to the formation of ANI^+. The inset emphasizes that direct attachment of ANI to PI within **1** both makes the reduction potential of PI more positive and makes that of NI more negative relative to the redox properties of these molecules within **2**. While the difference between the first reduction potentials of NI and PI within **1** is 180 mV, this differential increases to 330 mV in **2**. As will be shown below, this has a major impact on the electron-transfer dynamics observed for these compounds. The close proximity and cofacial arrangement of NI and PI in **1** and **2** has no observable impact on their redox properties. Additionally, replacement of the n-C_8H_{17} group in **2** with an H atom in **6** has no appreciable effect on the reduction potential of NI.

Time-Resolved Spectroscopy. Ultrafast transient absorption spectroscopy allows for direct observation of intermediate states formed during photoinduced charge separation reactions. Excitation of ANI within compounds **1**−**6** with 420 nm, 130 fs laser pulses results in formation of ^{1}*ANI, which can then transfer an electron to nearby acceptor groups. Within compound **1**, this results in formation of both the ANI^+−PI−NI^- and ANI^+−PI^-−NI ion pairs, as seen in Figure 3. Transient absorption measurements on **1** in toluene, MTHF, PrCN, and BzCN display spectral features characteristic of the NI^- anion radical[47] at 480 nm (ϵ = 28 300 $cm^{-1}M^{-1}$) and 605 nm (ϵ = 7000 $cm^{-1}M^{-1}$) as well as the 710 nm (ϵ = 41 700 $cm^{-1}M^{-1}$) spectral feature characteristic of the PI^- anion radical.[48,49] Monitoring the rise and decay of ΔA at these absorption maxima permits the direct determination of the time constants for charge separation (CS) and charge recombination (CR), which are listed for **1**−**6** in Tables 3 and 4, respectively. The ANI^+−PI−NI^- and ANI^+−PI^-−NI ion pairs within **1** both form and decay with very similar time constants, possibly indicative of a rapid equilibrium between them. Increasing the solvent polarity stabilizes the ion pairs and increases the free energy available for CS, while decreasing that for CR, resulting in faster rates for both processes, which is consistent with Marcus normal and inverted region behavior for CS and CR, respectively.[50] The ET dynamics are significantly different when a 2,5-dimethylphenyl bridge is inserted between ANI and PI in compound **2**. The transient absorption spectrum in Figure 3 shows that only the ANI^+−PI−NI^- ion pair is formed. There is no evidence for formation of the ANI^+−PI^-−NI ion pair. The CS and CR rates are also much slower than those observed within compound **1**. Transient absorption measurements on compounds **2** and **6** suggest that inverted kinetics, i.e., $k_{CS} < k_{CR}$ occur within these compounds in PrCN, and thus the time constant for CR cannot be measured.

In compounds **3** and **4** NI is replaced with NMI, which cannot be reduced by ^{1}*ANI. However, the steric interactions of NMI with PI are similar to those of NI with PI. In addition, the substituent effect of NMI on the xanthene spacer is similar to that of NI. Thus, a comparison between **1** and **3**, as well as between **2** and **4** can be made to assess the rate of transfer from ^{1}*ANI to PI alone, as well as ascertain the influence of the 2,5-dimethylphenyl spacer on the ET reaction. The transient absorption spectra of **1** and **2** are shown in Figure 3, while those of **3** and **4** are given in Figure 4. Comparing the results for **1** and **3**, ANI^+−PI^- forms in both molecules in all solvents; however, its rate of formation in **3** is three to seven times *slower* than in **1**. For example, a direct comparison of the transient absorption kinetics for the formation of the ANI^+−PI^- ion pair within **1** and **3** in toluene is shown in Figure 5. On the other hand, comparing the results for **2** and **4**, where a 2,5-dimethylphenyl group bridges ANI and PI, the ANI^+−PI^- ion

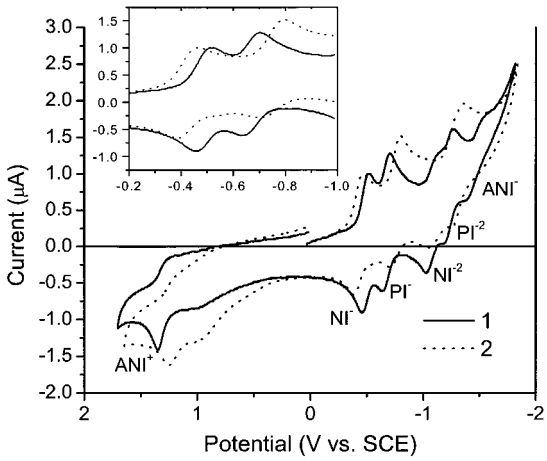

Figure 2. Cyclic voltammetry of **1** and **2** in 0.1 M tetra-n-butylammonium perchlorate PrCN solution. Scan rate 50 mV/s. Inset: First reduction waves of NI and PI within **1** and **2**.

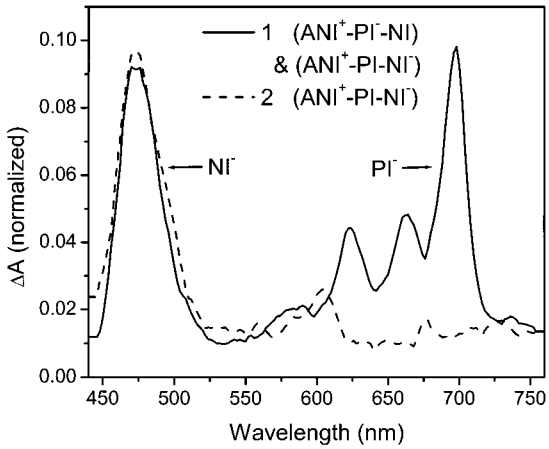

Figure 3. Transient absorption spectra of compounds **1** and **2** in toluene at t = 2 ns after excitation with a 420 nm, 130 fs laser pulse.

TABLE 3: CS Time Constants within Compounds 1−6 in the Solvents Specified

	τ_{CS} (ps)							
solvent	**1** (PI^-)	**1** (NI^-)	**2** (PI^-)	**2** (NI^-)	**3** (PI^-)	**4** (PI^-)	**5** (NI^-)	**6** (NI^-)
toluene	8.2	7.1	>8500	880	80	>8500	305	1200
MTHF	3.5	3.2	>7500	450	13	>7500	90	860
PrCN	3.0	2.5	>1500	480	5	>1500	50	630
BzCN	2.0	1.8	>3300	130	6	>3300	40	150

TABLE 4: CR Time Constants within Compounds 1−6 in the Solvents Specified

	τ_{CR} (ps)							
solvent	**1** (PI^-)	**1** (NI^-)	**2** (PI^-)	**2** (NI^-)	**3** (PI^-)	**4** (PI^-)	**5** (NI^-)	**6** (NI^-)
toluene	10000	13000		40000	3,500		20000	50000
MTHF	250	250		5000	575		2300	5000
PrCN	25	25		<480	30		140	<630
BzCN	50	60		460	80		200	450

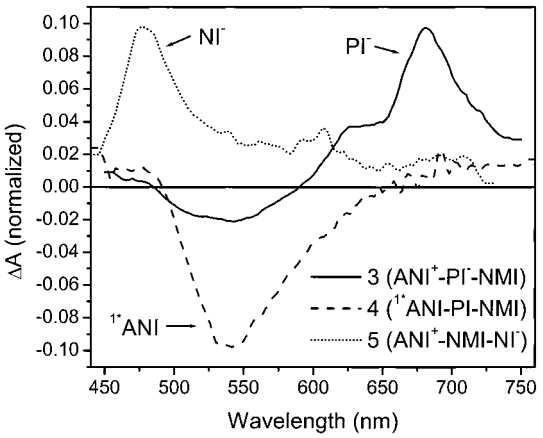

Figure 4. Transient absorption spectra of compounds **3** (—) and **5** (• •) in toluene at $t = 2$ ns after excitation with a 420 nm, 130 fs laser pulse which display spectra characteristic of the PI^- and NI^- anion radicals, respectively. Also shown is compound **4** (— —) in PrCN at $t = 5$ ns following excitation with a 420 nm, 130 fs laser pulse, displaying a spectrum characteristic of the ^{1}*ANI excited state.

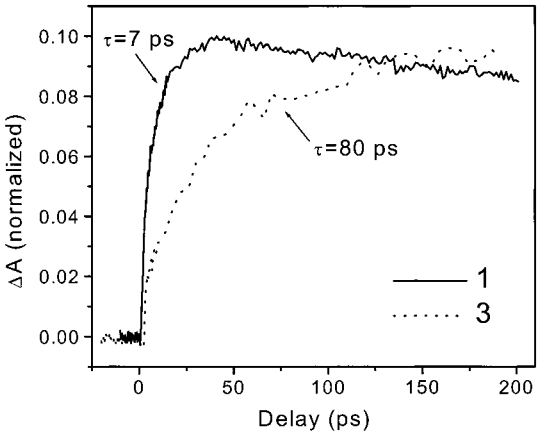

Figure 5. Transient kinetics monitoring formation of the ANI^+-PI^- ion pair at 710 nm within compounds **1** (—) and **3** (- -) following excitation with a 420 nm, 130 fs laser flash.

pair is not observed for either molecule in any solvent. This implies that the electron-transfer reaction ^{1}*ANI−PI → ANI^+-PI^- is most likely significantly slower than the excited-state decay of ^{1}*ANI under all conditions in **2** and **4**. Nevertheless, the formation of ANI^+-NI^- in **2** is clear from the intense NI^- signal at 480 nm in Figure 3. The transient absorption spectrum of **4** in Figure 4 displays only a positive ΔA near 450 nm due to ^{1}*ANI, and a negative ΔA between 490 and 550 nm due to stimulated emission from ^{1}*ANI, whose maximum is solvent dependent. These results strongly suggest that electron transfer from ^{1}*ANI to NI within **2** does not involve the ANI^+-PI^- intermediate.

Analogously, NMI can be substituted for PI within **2**, to produce compound **5**, wherein the through-space distance separating ANI and NI is slightly shorter than in **2** (13.6 versus 15.5 Å), while the donor−acceptor geometry is similar. The ET rates to form the ANI^+-NI^- ion pair in **5** reflect this shorter distance and are slightly *faster* than those observed within **2** in all solvents. Finally, both the CS and CR rates of compound **6** change relative to those of **2**, when an H atom is substituted for the n-C_8H_{17} chain of NI. The CS rates in toluene, MTHF, and PrCN are between 1.4 and 5.7 times faster when the n-C_8H_{17} chain is present in **2**. However, in BzCN the ET dynamics are identical within the two compounds.

TABLE 5: Donor−Acceptor Distances Obtained from Molecular Modeling Using MM+

compd	ANI−PI (Å)	ANI−NI (Å)
1	10.4	11.6
2	14.4	15.5
3	10.4	
4	14.4	
5		13.8
6		15.5

Discussion

Donor−Acceptor Orientation. The xanthene scaffold rigidly positions the donor−acceptor components such that their primary degrees of orientational freedom are torsional motions around the single bonds joining them. Geometry optimization calculations at the AM1 level of theory were performed to determine donor−acceptor distances and torsional angles within **1**−**6**.[51] The results show that the torsional angles between the π systems of NI and/or PI and that of the xanthene scaffold are 60−80° within **1**−**6**. This positions the acceptor moieties cofacially, with 4.5−4.7 Å separating the average planes of their π systems. This suggests that there is insufficient space for solvent molecules to fit between the acceptors in any of the compounds. Despite their close proximity the photophysical and electrochemical properties of NI and PI remain essentially unperturbed. The orientation of ANI relative to PI and NI depends on the presence or absence of the 2,5-dimethylphenyl bridging group. Direct attachment of ANI to PI via an imide−imide bond in **1** and **3** results in approximately a 60° torsional angle between the π-systems of ANI and PI. The 2,5-dimethylphenyl bridge adopts 90° torsional angles with respect to both imides in **2**, **4**, and **6**. Thus, the π-system of ANI lies in the same plane as that of PI within these compounds. The phenyl bridge within **5** is an intermediate case, adopting torsional angles of approximately 60° relative to both NMI and ANI.

Ion Pair Energies. An accurate assessment of the ion pair energies is critical to elucidating the mechanisms for CS and CR within **1**−**6**, and can be particularly difficult in low polarity media such as toluene. Previously, the high degree of charge separation within the ^{1}*ANI excited state was used to calculate the energies of successively formed ion pair states by treating electron transfer from ^{1}*ANI to the acceptor as a charge shift reaction.[24] The energies of the ion pair states within **1**−**6** in toluene and MTHF are calculated using the relationship:

$$\Delta G_{IP} = E_S + E_{RED,ANI} - E_{RED,ACC} + \frac{e^2}{\epsilon_s}\left(\frac{4.8q^3}{\mu} - \frac{1}{r_{DA}}\right) \quad (1)$$

where E_S is the excited-state energy of ANI (Table 1), $E_{RED,ANI}$, and $E_{RED,ACC}$ are the reduction potentials of ANI and the PI or NI acceptor (Table 2), e is the fundamental charge, q is the fractional degree of charge separation within ^{1}*ANI ($q = 0.7$), μ is the excited-state dipole moment of ^{1}*ANI (11.1 D), and r_{DA} is the charge separation distance within the donor−acceptor ion pair, Table 5. The ion pair energies in PrCN and BzCN were calculated directly using the oxidation and reduction potentials of the donor and acceptor, respectively, and the Coulomb stabilization of the ion pair:

$$\Delta G_{IP} = E_{OX} - E_{RED} - \frac{e^2}{\epsilon_s r_{DA}} \quad (2)$$

The free energies for CS and CR listed in Table 3 are calculated using

$$\Delta G_{CS} = \Delta G_{IP} - E_S \quad (3)$$

$$\Delta G_{CR} = -\Delta G_{IP} \quad (4)$$

Charge separation to NI and/or PI is thermodynamically favorable within **1**−**6** in all solvents, as listed in Table 6. The difference in free energy for CS to PI versus NI within compounds **1** and **2** is dictated largely by the disparity in their reduction potentials, and to a lesser degree, by changes in the Coulombic stabilization energy arising from different ion pair distances. Within **1**, the difference between the first reduction potentials of NI and PI is 0.18 V, while within **2**, it is 0.33 V. Thus, the calculated difference in free energy between the $ANI^+-PI-NI^-$ and ANI^+-PI^--NI ion pairs within **1** is only about 0.1 eV, which is approximately the error within this calculation, while within **2**, ANI^+-PI^--NI is 0.3 eV less stable than is $ANI^+-PI-NI^-$. Energy level diagrams for compounds **1** and **2** in toluene are displayed in Figures 6 and 7.

Charge Separation and Recombination Mechanisms. The most likely mechanisms for the formation of $ANI^+-PI-NI^-$ within **1** and **2** are sequential electron transfer and superexchange. These possibilities will each be considered separately in the following discussion. The sequential electron-transfer mechanism involves the reactions: ^{1}*ANI−PI−NI → ANI^+-PI^--NI → $ANI^+-PI-NI^-$. On the other hand, superexchange mechanisms for the formation of $ANI^+-PI-NI^-$ are more complex because they can make use of pathways through the covalent bonds linking ^{1}*ANI and NI, as well as interactions between ^{1}*ANI and groups that are not directly bonded to ^{1}*ANI, such as the *n*-C_8H_{17} alkyl tail on molecules **1**, **2**, and **5** or solvent molecules that are positioned between ^{1}*ANI and NI.

To determine whether the sequential mechanism is operative, compounds **3** and **4** were prepared as reference molecules to obtain the rate of the reaction ^{1}*ANI−PI−NI → ANI^+-PI^-−NI in **1** and **2**, respectively. In both **3** and **4** the NI acceptor is replaced with NMI, the reduction potential of which is −1.4 V vs SCE, so that NMI cannot be reduced by ^{1}*ANI in any of the solvents examined, and PI is the only viable electron acceptor. Importantly, the ion pair distances and free energies for the formation of ANI^+-PI^- are the same in **1** and **3**, as well as in **2** and **4**. Photoexcitation of both **1** and **3** produces ANI^+-PI^-. Yet, depending on the solvent, the rate of ANI^+-PI^- formation within **1** is 2−10 times *faster* than the rate of ANI^+-PI^- formation within **3**. Moreover, the rates of formation of both ANI^+-PI^- and ANI^+-NI^- within **1** are the same within experimental error. These facts strongly suggest that the formation of $ANI^+-PI-NI^-$ within **1** is not *preceded* by the formation of ANI^+-PI^--NI. On the other hand, the data for **1** support the reaction sequence ^{1}*ANI−PI−NI → $ANI^+-PI-NI^-$ → ANI^+-PI^--NI. The calculated free energies given in Table 6 and illustrated in Figure 6 show that the ANI^+-PI^--NI and $ANI^+-PI-NI^-$ ion pairs in **1** are nearly isoenergetic, so that it is possible that they are in rapid equilibrium. This is also supported by the CR rates within **1**, which show that ANI^+-PI^--NI and $ANI^+-PI-NI^-$ decay with similar rates in all the solvents examined.

A comparison of the ET dynamics within **2** and **4** provides evidence against sequential electron-transfer involving the formation ANI^+-PI^--NI in **2** as well. The ANI^+-PI^- ion pair is not formed within **2** and **4** in any of the four solvents studied, as evidenced by both the steady-state emission quantum yields and transient absorption spectra, despite favorable free energies greater than −0.6 eV in the nitrile solvents. This is presumably

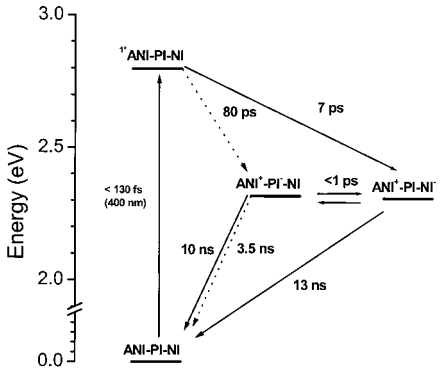

Figure 6. Energy level diagram and time constants for formation of the ion pairs within compound **1** (—) in toluene. Also shown for comparison are time constants for formation and decay of the ANI^+-PI^--NMI ion pair within **3** (- -) in toluene.

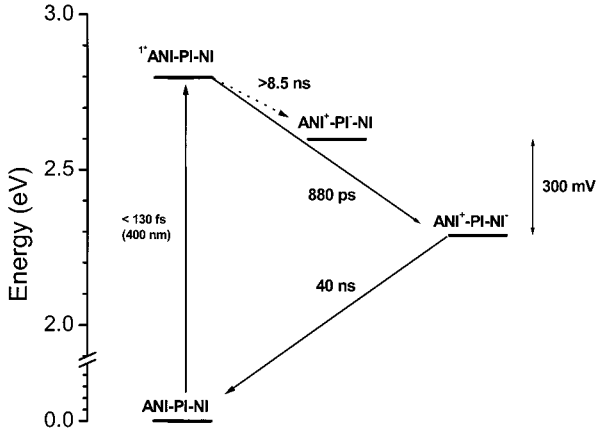

Figure 7. Energy level diagram and rate constants for formation of ion pairs within compound **2** in toluene.

TABLE 6: Free Energies for CS (eV) within Compounds 1−6 Calculated Using Equation 1

solvent	**1** (PI^-)	**1** (NI^-)	**2** (PI^-)	**2** (NI^-)	**3** (PI^-)	**4** (PI^-)	**5** (NI^-)	**6** (NI^-)
toluene	−0.37	−0.49	−0.21	−0.51	−0.38	−0.22	−0.55	−0.49
MTHF	−0.58	−0.70	−0.53	−0.83	−0.59	−0.54	−0.85	−0.83
PrCN	−0.66	−0.78	−0.64	−0.94	−0.67	−0.65	−0.97	−0.95
BzCN	−0.66	−0.78	−0.64	−0.95	−0.67	−0.65	−0.97	−0.95

a consequence of the decreased electronic coupling matrix element for ET from ^{1}*ANI to PI due to the insertion of the 2,5-dimethylphenyl spacer in **2** and **4**. The π system of this spacer is approximately perpendicular to those of both ANI and PI, so that only the high-lying σ* orbitals of the spacer are available to interact with the π systems of ^{1}*ANI and PI. The fluorescence quantum yields for **4** display the same solvent dependence as observed for the ANI chromophore alone. The small degree of quenching in **4** most likely arises from nonradiative decay processes intrinsic to the molecule, which have no solvent dependence. Despite the fact that there is no evidence for the formation of ANI^+-PI^--NI following photoexcitation of **2**, $ANI^+-PI-NI^-$ does form on a subnanosecond time scale in all the solvents examined. While rapid equilibrium between $ANI^+-PI-NI^-$ and ANI^+-PI^--NI is established within **1**, this does not occur within **2** because the free energy difference between ANI^+-PI^--NI and $ANI^+-PI-NI^-$ is about 0.3 eV, as seen from the data in Table 6 and illustrated in the energy level diagram in Figure 7. Our data do not support the sequential electron-transfer mechanism for CS within **1** and **2**, which requires that ANI^+-PI^--NI is formed *prior* to $ANI^+-PI-NI^-$.

Superexchange mechanisms of electron transfer within **1**-**6** will now be discussed in detail. In a typical donor-bridge-acceptor (D−B−A) molecule the superexchange mechanism for electron transfer involves mixing of electronic states of the bridge molecule with those of the donor and acceptor. This mixing depends critically on both the spatial overlap of the molecular orbitals of B with those of D and A, and the vertical energy gap between the ^{1}*D−B−A excited state and the energetically higher lying D^+-B^--A state.[52] In principle, several different states of B can contribute to the overall electronic coupling between ^{1}*D and A, their relative contributions being determined by the electronic couplings and the energy gaps between the various states.[53−55] In addition, several different bridging groups within a single donor−acceptor array can serve to mediate ET between the donor and the acceptor. The free energies for CS listed in Table 6 show that the ANI^+-PI^--NI ion pair state within **1** and **2** is energetically below that of ^{1}*ANI in all the solvents studied, so that the ANI^+-PI^--NI ion pair state cannot be involved in any superexchange electron-transfer mechanism that produces $ANI^+-PI-NI^-$.

Compound **5** was prepared to examine superexchange interactions by replacing the PI acceptor with NMI, which is about 0.7 V harder to reduce, and places the energy of ANI^+-NMI^--NI above that of ^{1}*ANI in all the solvents studied. The ANI−NI center-to-center, through-space distance in **5** decreases by 2 Å relative to that in **2**, while the calculated energy of the ANI^+-NI^- ion pair state in **5** is 20−40 meV lower than that of **2** depending on solvent, Table 6. The CS rates for the reaction ANI−NI → ANI^+-NI^- and the CR rates for the reaction ANI^+-NI^- → ANI−NI within **5** (Tables 3 and 4) are both only 2−10 times faster than those observed for the same reactions within **2** in all solvents. This suggests that the rate changes observed between **2** and **5** can be accounted for in a straightforward fashion by the small changes in the ANI−NI through-space distance and ANI^+-NI^- energy, and further supports the idea that the mechanism for CS and CR within **1** and **2** most likely involve a superexchange-mediated interaction between ^{1}*ANI and NI (mechanisms B and C, Scheme 1).

The question remains as to which virtual states of these molecules contribute to the overall electron-transfer process. The data for **1**, **2**, and **5** point to a superexchange mechanism of electron transfer possibly involving the *n*-C_8H_{17} aliphatic chain attached to the nitrogen of the imide of NI as well as solvent molecules occupying the space between ^{1}*ANI and NI (mechanism C, Scheme 1). In addition, the σ* orbitals of the phenyl spacers within **2** and **5** could contribute. It is unlikely that the long through-bond pathway between ANI and NI contributes significantly (mechanism A, Scheme 1), especially in light of the fact that the presence of the 2,5-dimethylphenyl spacer in **2** and **4** makes electron transfer to PI noncompetitive with excited-state decay of ^{1}*ANI.

The energies of the frontier MOs localized on a *n*-C_8H_{17} aliphatic chain, as well as those of the relevant solvent molecules were calculated using the AM1 model and are shown in Figure 8. The energies of the σ* orbitals of the phenyl spacers within **2** and **5** have very similar energies to those of the *n*-C_8H_{17} aliphatic chain. As expected, these calculations show that the lowest unoccupied orbital localized on the *n*-C_8H_{17} aliphatic chain has a reasonably high energy. In addition, the calculations show that the energies of the π symmetric LUMOs of toluene and BzCN are both low, and the overall ordering of LUMO energies for the solvents is BzCN < toluene < PrCN < MTHF. Previous work on medium-mediated ET has demonstrated a correlation between the vertical electron affinity of the solvent

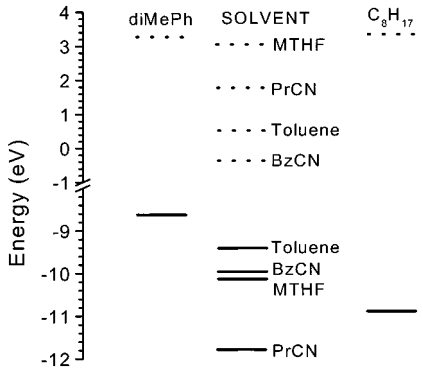

Figure 8. Energy level diagram featuring the frontier orbitals of the media contributing to superexchange.

(EA_V) and the magnitude of electronic coupling mediated by a D^+-S^--A virtual state.[32,33,37] A general comparison can be made between LUMO energy and EA_V.[56] Of the solvents employed here, a direct comparison can be made between BzCN and PrCN, whose dielectric constants are nearly identical, resulting in similar driving force for CS, but which differ considerably in EA_V values. While little change in the CS rates within **1** or **5** is observed between PrCN and BzCN, the rates of CS differ considerably within **2**. This change in CS rates within the nitrile solvents is also observed within compound **6**, in which the *n*-C_8H_{17} aliphatic chain is removed from NI and replaced with a hydrogen atom. These observations suggest that within **2** and **6** CS may be mediated in part by an ANI^+-BzCN^--NI virtual state, while the LUMO energies of the other solvents are not sufficiently low to provide states that mediate ET effectively. Unfortunately, no comparison can be made regarding solvent mediation of CR between PrCN and BzCN because the CS and CR kinetics of **2** and **6** within PrCN are inverted, i.e., $k_{CS} < k_{CR}$.

The flexible *n*-C_8H_{17} aliphatic chain on NI within **1**, **2**, and **5** occupies space between ANI and NI that would otherwise be occupied by additional solvent molecules, and its removal should accentuate the role solvent can play in mediating electron transfer from ^{1}*ANI to NI. Direct comparisons can be made between **2** and **6** because their structures differ only by the presence or absence of the *n*-C_8H_{17} tail. Their redox properties and donor−acceptor distances and orientations are unchanged. In addition, the contribution of the phenyl spacer to a superexchange interaction is also constant in **2** and **6**. Steady-state and transient absorption measurements show that CS occurs readily within **6** in all solvents. However, the CS rates within **2**, where *n*-C_8H_{17} is present, are factors of 1.4, 1.9, 1.3, and 1.1 times *faster* in toluene, MTHF, PrCN, and BzCN respectively, relative to those within **6**, where *n*-C_8H_{17} is absent. These data are best explained by invoking a modest overall contribution of the *n*-C_8H_{17} chain to a superexchange interaction mediating ^{1}*ANI to NI electron transfer that is competitive with solvent-mediated superexchange (mechanism C, Scheme 1). Contributions from the solvent are expected to be weak generally because it is unlikely that the orientations of the solvent molecules relative to ANI and NI are fixed in geometries especially conducive to mediating ET in these systems. Moreover, it is not possible to separate the superexchange ineraction involving the solvent from the direct, through-space interaction between ^{1}*ANI and NI (mechanism B, Scheme 1). Solvent-mediated ET has been previously observed only within U-shaped D−B-A molecules containing a cleft between D and A for single solvent molecules to enter between the chromophores.[26,32−37]

The solvent with the weakest ability to mediate CS, i.e., the highest lying LUMO, MTHF, exhibits the greatest difference in rates when the aliphatic chain is removed, while the rates are nearly identical in BzCN. This suggests that the role of the aliphatic chain in mediating ET becomes more important when the solvent cannot readily participate in superexchange. Conversely, its role is diminished in solvents with low energy LUMOs that provide an energetically facile superexchange pathway for electron transfer. Why is the *n*-C_8H_{17} chain effective at mediating ET even though its LUMO is as high as that of MTHF? We suggest that covalently attaching the *n*-C_8H_{17} chain to the imide nitrogen atom of NI constrains the chain to be close to ^{1}*ANI, resulting in a short average distance between ^{1}*ANI and *n*-C_8H_{17} that increases the electronic coupling matrix element for the direct, through-space interaction (mechanism C, Scheme 1). Moreover, the short, through-bond coupling pathway within *n*-C_8H_{17} can then provide an ET pathway to NI. While it is difficult to speculate on the orientation of one or more solvent molecules, which contribute to the electronic coupling between ^{1}*ANI and NI in **6,** the imide N−H could provide a potential site for weak hydrogen bonding with the nitrile group in PrCN and BzCN. Further studies are underway to quantify the contribution of solvent to the overall electronic coupling within these and similar compounds.

Distance Dependence of Medium-Mediated Superexchange. Compounds **1**, **2**, and **5** most likely undergo ET via a superexchange mechanism mediated by the *n*-C_8H_{17} chain of NI and the solvent between ANI and NI. While limited torsional motion can occur around the single bonds linking the various aromatic components, the ANI−NI distance changes systematically among these three compounds. If one assumes that the exponential dependence of the electronic coupling is dominant over all other distance dependencies, then the rate of nonadiabatic electron transfer described by Fermi's Golden Rule[57−59] can be expressed as

$$k_{ET} = A(T)e^{-\beta r_{DA}}$$

in which $A(T)$ is a temperature-dependent prefactor that incorporates all the contributions to k_{ET} arising from the thermodynamic driving force, Franck−Condon factors, vibrations, and solvent polarization, and β is a parameter with units of inverse length, which characterizes the steepness of the exponential distance dependence of k_{ET}. Plotting the natural logarithm of the CS and CR rates versus the ANI−NI donor−acceptor distance in Figure 9, parts a and b, respectively, yields a linear distance dependence in all four solvents. The linear dependence observed for CR in PrCN is trivialized as a consequence of only two available data points. The D−A distance for CS is approximately 5 Å shorter than that for CR because CS is essentially a charge shift reaction from the aromatic imide of ANI to NI while the positive charge density within ANI^+ resides predominantly on the nitrogen atom of the piperidine ring of ANI.

The β values ($Å^{-1}$) determined by linear least-squares fits to the natural log of the CS rates are listed in Table 7. Toluene and MTHF exhibit the sharpest distance dependence, although the β values for all four solvents are all in the range of 1.1−1.3 $Å^{-1}$. These values are in agreement with previously published values for ET across saturated aliphatic bridges, $\beta = 0.7-1.2$ $Å^{-1}$,[60−63] and through-space ET between cofacial porphyrin and quinone molecules, $\beta = 1.3$ $Å^{-1}$.[38] The relative values of β calculated for the four solvents also agree well with the ordering of LUMO energies of the solvents, with BzCN as the best mediator of CS.

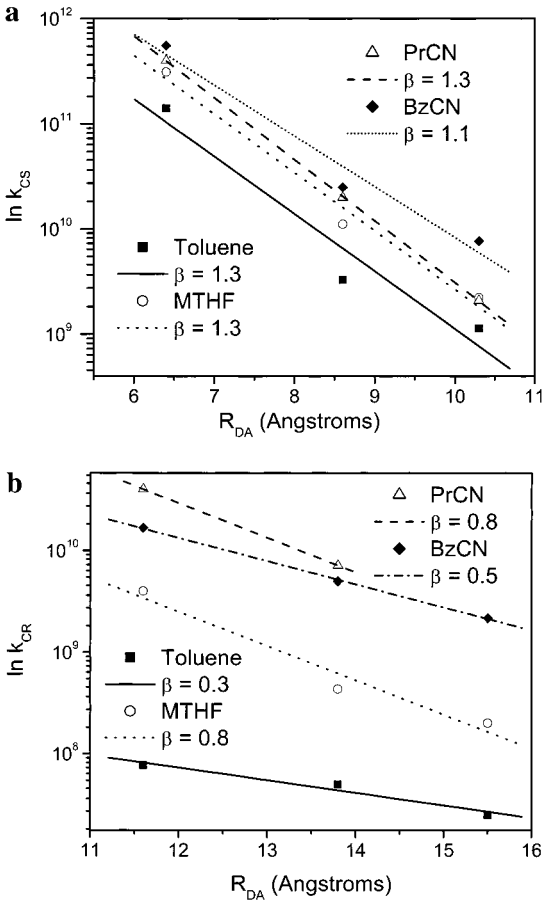

Figure 9. Distance dependence of CS (A) and CR (B) rates for the ANI^+-NI^- ion pair within compounds **1**, **2**, and **5**.

TABLE 7: Distance Dependence of CS and CR within Compounds 1, 2, and 5

solvent	CS β ($Å^{-1}$)	CR β ($Å^{-1}$)
toluene	1.3	0.3
MTHF	1.3	0.8
PrCN	1.3	0.8
BzCN	1.1	0.5

The distance dependence of CR is more strongly influenced by solvent than is CS. The most dramatic example is that of toluene, where $\beta_{CS} = 1.3$ $Å^{-1}$, while $\beta_{CR} = 0.3$ $Å^{-1}$. This is best explained by mechanistic differences between CS and CR. While CS must occur by moving an electron from ^{1}*D to A, and should reflect the energy of the LUMOs that mediate superexchange, CR can occur via either electron or hole transfer. Thus, both HOMOs and LUMOs can contribute to mediation of CR. The orbital energy data in Figure 8 suggests that toluene should be the best mediator for CR via a hole-transfer mechanism. Once again the order of frontier orbital energies of the solvents is reflected in the ability of the solvent to mediate ET, with the aliphatic solvents PrCN and MTHF being the poorest at facilitating ET.

Conclusions

The ET dynamics observed within **1**−**6** indicate that CS between ANI and NI occurs by superexchange interactions that include contributions from the *n*-C_8H_{17} substituent on the NI acceptor and solvent molecules. The structural rigidity of these compounds allows evaluation of the distance dependencies of both CS and CR. For CS, $\beta = 1.1-1.3$ $Å^{-1}$, and evidence exists for solvent contributions to superexchange in BzCN. The

distance dependence of CR rates also correlates strongly with contributions from solvent molecules mediating this process via a hole-transfer mechanism in toluene. Once again the aromatic solvents toluene and BzCN display the best ability to mediate ET via superexchange. Our findings indicate that mediation of electron transfer by nonbonded interactions can compete with electron transfer via bonded pathways. We are carrying out further studies in an attempt to quantify the contributions from through-bond and through-space interactions to the electronic coupling between electron donors and acceptors.

Acknowledgment. This work was supported by the Division of Chemical Sciences, Office of Basic Research, U.S. Department of Energy, Grant DE-FG02-99ER14999.

Supporting Information Available: Synthetic and spectroscopic details. This material is available free of charge via the Internet at http://www.pubs.acs.org.

References and Notes

(1) Deisenhofer, J.; Epp, O.; Miki, K.; Huber, R.; Michel, H. *J. Mol. Biol.* **1984**, *180*, 385−398.
(2) Kirmaier, C.; Holten, D. *Proc. Natl. Acad. Sci. U.S.A.* **1990**, *87*, 3552−3556.
(3) Holzapfel, W.; Finkele, U.; Kaiser, W.; Oesterhelt, D.; Scheer, H.; Stilz, H. U.; Zinth, W. *Chem. Phys. Lett.* **1989**, *160*, 1−7.
(4) Martin, J. L.; Breton, J.; Hoff, A. J.; Migus, A.; Antonetti, A. *Proc. Natl. Acad. Sci. U.S.A.* **1986**, *83*, 957.
(5) Bixon, M.; Jortner, J.; Michel-Beyerle, M. E. *Biochim. Biophys. Acta* **1991**, *1056*, 301−315.
(6) Kirmaier, C.; Holten, D. In *The Photosynthetic Reaction Center*; Deisenhofer, J., Norris, J. R., Eds.; Academic Press: San Diego, 1993; Vol. 2, pp 49−71.
(7) Ogrodnik, A.; Michel-Beyerle, M. E. *Z. Naturforsch.* **1989**, *44a*, 763−764.
(8) DiMagno, T. J.; Norris, J. R. In *The Photosynthetic Reaction Center*; Deisenhofer, J., Norris, J. R., Eds.; Academic Press: San Diego, 1993; Vol. 2, pp 105−133.
(9) Sumi, H.; Kakitani, T. *Chem. Phys. Lett.* **1996**, *252*, 85−93.
(10) Plato, M.; Mobius, K.; Michel-Beyerle, M. E.; Bixon, M.; Jortner, J. *J. Am. Chem. Soc.* **1988**, *110*, 7279−7285.
(11) Allen, J. P.; Feher, G.; Yeates, T. O.; Komiya, H.; Rees, D. C. *Proc. Natl. Acad. Sci. U.S.A.* **1987**, *84*, 5730−5734.
(12) Yeates, T. O.; Komiya, H.; Chiring, D. C.; Rees, D. C.; Allen, J. P.; Feher, G. *Proc. Natl. Acad. Sci. U.S.A.* **1988**, *85*, 7993−7997.
(13) Sessler, J. L.; Johnson, M. R.; Lin, T.-Y. *Tetrahedron* **1989**, *45*, 4767−4784.
(14) Kuciauskas, D.; Liddell, P. A.; Hung, S.-C.; Lin, S.; Stone, S.; Seely, G. R.; Moore, A. L.; Moore, T. A.; Gust, D. *J. Phys. Chem. B* **1997**, *101*, 429−440.
(15) Wasielewski, M. R.; Niemczyk, M. P.; Johnson, D. G.; Svec, W. A.; Minsek, D. W. *Tetrahedron* **1989**, *45*, 4785−4806.
(16) Wiederrecht, G. P.; Watanabe, S.; Wasielewski, M. R. *Chem. Phys.* **1993**, *176*, 601−614.
(17) Johnson, D. G.; Niemczyk, M. P.; Minsek, D. W.; Wiederrecht, G. P.; Svec, W. A.; Gaines, G. L., III.; Wasielewski, M. R. *J. Am. Chem. Soc.* **1993**, *115*, 5692−5701.
(18) Osuka, A.; Marumo, S.; Mataga, N.; Taniguchi, S.; Okada, T.; Yamzaki, I.; Nishimura, Y.; Ohno, T.; Nozaki, K. *J. Am. Chem. Soc.* **1996**, *118*, 155-167.
(19) Osuka, A.; Mataga, N.; Okada, T. *Pure Appl. Chem.* **1997**, *69*, 797−802.
(20) Oevering, H.; Paddon-Row, M. N.; Heppener, M.; Oliver, A. M.; Cotsaris, E.; Verhoeven, J. W.; Hush, N. S. *J. Am. Chem. Soc.* **1987**, *109*, 3258−3269.
(21) Rodriguez, J.; Kirmaier, C.; Johnson, M. R.; Friesner, R. A.; Holten, D.; Sessler, J. L. *J. Am. Chem. Soc.* **1991**, *113*, 1652−1659.
(22) Wasielewski, M. R. *Chem. Rev.* **1992**, *92*, 435−461.
(23) Lee, S.-J.; DeGraziano, J. M.; Macpherson, A. N.; Shin, E.-J.; Kerrigan, P. K.; Seely, G. R.; Moore, A. L.; Moore, T. A.; Gust, D. *Chem. Phys.* **1993**, *176*, 321−326.
(24) Greenfield, S. R.; Svec, W. A.; Gosztola, D.; Wasielewski, M. R. *J. Am. Chem. Soc.* **1996**, *118*, 6767−6777.
(25) Gosztola, D.; Wang, B.; Wasielewski, M. R. *J. Photochem. Photobiol. A: Chem.* **1996**, *102*, 71−80.
(26) Jolliffe, K. A.; Bell, T. D. M.; Ghiggino, K. P.; Langford, S. J.; Paddon-Row, M. N. *Angew. Chem., Int. Ed. Engl.* **1998**, *37*, 916−919.
(27) Seischab, M.; Lodenkemper, T.; Stockmann, A.; Schneider, S.; Koeberg, M.; Roest, M. R.; Verhoeven, J. W.; Lawson, J. M.; Paddon-Row: M. N. *Phys. Chem. Chem. Phys.* **2000**, *2*, 1889−1897.
(28) Lokan, N. R.; Paddon-Row, M. N.; Koeberg, M.; Verhoeven, J. W. *J. Am. Chem. Soc.* **2000**, *122*, 5075−5081.
(29) Armspach, D.; Matt, D.; Harriman, A. *Eur. J. Inorg. Chem.* **2000**, *6*, 1147−1150.
(30) Hu, Y.-Z.; Bossmann, S. H.; van Loyen, D.; Schwarz, O.; Durr, H. *Chem. Eur. J.* **1999**, *5*, 1267−1277.
(31) Linke, M.; Chambron, J.-C.; Heitz, V.; Sauvage, J.-P. *J. Am. Chem. Soc.* **1997**, *119*, 11329−11330.
(32) Kumar, K.; Lin, Z.; Waldeck, D. H.; Zimmt, M. B. *J. Am. Chem. Soc.* **1996**, *118*, 243−244.
(33) Han, H.; Zimmt, M. B. *J. Am. Chem. Soc.* **1998**, *120*, 8001−8002.
(34) Lawson, J. M.; Paddon-Row, M. N.; Schuddeboom, W.; Warman, J. M.; Clayton, A. H. A.; Ghiggino, K. P. *J. Phys. Chem.* **1993**, *97*, 13099−13106.
(35) Head, N. J.; Oliver, A. M.; Look, K.; Lokan, N. R.; Jones, G. A.; Paddon-Row, M. N. *Angew. Chem., Int. Ed. Engl.* **1999**, *38*, 3219−3222.
(36) Bell, T. D. M.; Jolliffe, K. A.; Ghiggino, K. P.; Oliver, A. M.; Shepard, M. J.; Langford, S. J.; Paddon-Row, M. N. *J. Am. Chem. Soc.* **2000**, *122*, 10661−10666.
(37) Kaplan, R. W.; Napper, A. M.; Waldeck, D. H.; Zimmt, M. B. *J. Am. Chem. Soc.* **2000**, *122*, 12039−12040.
(38) Lindsey, J. S.; Delaney, J. K.; Mauzerall, D. C.; Linschitz, H. *J. Am. Chem. Soc.* **1988**, *110*, 3610−3621.
(39) Higashida, S.; Tsue, H.; Sugiura, K.-i.; Kaneda, T.; Sakata, Y.; Tanaka, Y.; Taniguchi, S.; Okada, T. *Bull. Chem. Soc. Jpn.* **1996**, *69*, 1329−1335.
(40) Staab, H. A.; Nikolic, S.; Krieger, C. *Eur. J. Org. Chem.* **1941**, *6*, 1459−1470.
(41) Guldi, D. M.; Luo, C.; Da Ros, T.; Prato, M.; Dietel, E.; Hirsch, A. *Chem. Commun.* **2000**, 375−376.
(42) Burrow, P. D.; Howard, A. E.; Johnston, A. R.; Jordan, K. D. *J. Phys. Chem.* **1992**, *96*, 7570−7578.
(43) Hamann, B. C.; Branda, N. R.; Rebek, J., Jr. *Tetrahedron Lett.* **1993**, *34*, 6837−6840.
(44) Lukas, A. S.; Miller, S. E.; Wasielewski, M. R. *J. Phys. Chem. B* **2000**, *104*, 931−940.
(45) Miller, S. E.; Schaller, R.; Mulloni, V.; Zhao, Y.; Just, E. M.; Johnson, R. C.; Gosztola, D.; Wasielewski, M. R. *J. Phys. Chem. B* **2001**. Submitted for publication.
(46) Viehbeck, A.; Goldberg, M. J.; Kovac, C. A. *J. Electrochem. Soc.* **1990**, *137*, 1460−1466.
(47) Wiederrecht, G. P.; Niemczyk, M. P.; Svec, W. A.; Wasielewski, M. R. *J. Am. Chem. Soc.* **1996**, *118*, 81−88.
(48) Osuka, A.; Nakajima, S.; Maruyama, K.; Mataga, N.; Asahi, T. *Chem. Lett.* **1991**, 1003−1006.
(49) Gosztola, D.; Niemczyk, M. P.; Svec, W. A.; Lukas, A. S.; Wasielewski, M. R. *J. Phys. Chem. A* **2000**, *104*, 6545−6551.
(50) Marcus, R. A. *J. Chem. Phys.* **1965**, *43*, 679−701.
(51) Ion pair distances were estimated from structures calculated using the MM+ force field and AM1 MO calculations performed within HyperChem(TM) V5.01a, Hypercube, Inc., 1115 NW 4th Street, Gainesville, FL 32601.
(52) McConnell, H. M. *J. Chem. Phys.* **1961**, *35*, 508−515.
(53) Kuznetsov, A. M.; Ulstrup, J. *J. Chem. Phys.* **1981**, *75*, 2047−2055.
(54) Tang, J.; Wang, Z.; Norris, J. R. *J. Chem. Phys.* **1993**, *99*, 979−984.
(55) Tang, J.; Norris, J. R. *J. Chem. Phys.* **1994**, *101*, 5615−5622.
(56) Burrow, P. D.; Howard, A. E.; Johnston, A. R.; Jordan, K. D. *J. Phys. Chem.* **1992**, *96*, 7570−7578.
(57) Devault, D. *Quantum Mechanical Tunneling in Biological Systems*; Cambridge University Press: Cambridge, 1984.
(58) Newton, M. D.; Sutin, N. *Annu. Rev. Phys. Chem.* **1984**, *35*, 437−480.
(59) Marcus, R. A.; Sutin, N. *Biochim. Biophys. Acta* **1985**, *811*, 265−322.
(60) Paddon-Row, M. N.; Oliver, A. M.; Warman, J. M.; Smit, K. J.; de Haas, M. P.; Oevering, H.; Verhoeven, J. W. *J. Phys. Chem.* **1988**, *92*, 6958−6962.
(61) Sachs, S. B.; Dudek, S. P.; Hsung, R. P.; Sita, L. R.; Smalley, J. F.; Newton, M. D.; Feldberg, S. W.; Chidsey, C. E. D. *J. Am. Chem. Soc.* **1997**, *119*, 10563−10564.
(62) Park, J. W.; Lee, B. A. L.; Lee, S. Y. *J. Phys. Chem. B* **1998**, *102*, 8209−8215.
(63) Le, T. P.; Rogers, J. E.; Kelly, L. A. *J. Phys. Chem. A* **2000**, *104*, 6778−6785.